NJC

PAPER

View Article Online
View Journal | View Issue

Cite this: *New J. Chem.*, 2018, 42, 18288

Synthesis of poly(α-olefins) containing rare short-chain branches by dinuclear Ni-based catalysts†

M. Khoshsefat, [ab] A. Dechal,[a] S. Ahmadjo, *[a] S. M. M. Mortazavi,[a] G. H. Zohuri[c] and J. B. P. Soares[b]

Received 3rd September 2018,
Accepted 1st October 2018

DOI: 10.1039/c8nj04481c

rsc.li/njc

1-Hexene homopolymer samples produced by a series of mononuclear (MC_n, n = 1–3) and rigid/flexible bridged dinuclear (BC_n, n = 1–7) Ni-based catalysts were characterized by ^{13}C NMR, DSC, and GPC-IR analyses. Mononuclear catalysts through normal insertion produced poly(1-hexene) with a high amount of butyl branches, while dinuclear catalysts were able to polymerize 1-hexene with a high level of rare branches (ethyl and propyl) due to the partial chain walking mechanism. Theoretical calculation was employed in order to study the dinuclear catalysts, which confirmed the presence of two stereoisomers *via* the broadening of MWD, a different mechanism of polymerization and short chain branch (SCB) curves. The effects of the cocatalyst type (DEAC, EASC and MMAO) and concentration, time and temperature along with the polymerization of higher α-olefins (1-octene and 1-decene) on the behavior of dinuclear catalyst BC_2 and polymer properties were investigated. As a result, in addition to catalyst structure, the monomer length and polymerization temperature were the two factors controlling the stability of the stereoisomers due to agostic interaction and kinetic energy, respectively.

Introduction

Recently, the (co)polymerization of long α-olefins and functional monomers besides ethylene and propylene have captured the attention of researchers and readers.[1–5] This attention is due to the long chain α-olefins and the polarity of the functional comonomers that has a remarkable effect on catalyst behaviour and polymer properties such as tensile strength, strain, and wettability.[6–10] These α-olefins have been polymerized using different types of catalysts from commercial to novel lab-scale catalysts.[11–17] Moreover, catalyst structure along with the polymerization parameters led to the production of amorphous to semi-crystalline polymers. With regard to catalyst architecture, multinuclearity as well as the ligand steric and electronic effects are important factors affecting catalyst behaviour.[10,17–27]

The chain walking polymerization of α-olefins is pronounced using a different structure of mononuclear Ni and Pd catalysts. However, there is a demand for the investigation of the effect of nuclearity on the mechanism of polymerization by multinuclear catalysts. In addition, the monomer length in regard to the agostic interaction as well as the distance between the active centers are important.[12,21,23,28–31] The (co)polymerization of long α-olefins, as previously mentioned, can be beneficial to better understand the synergistic and cooperative effects. These effects could be observed when catalytic behavior or polymer properties are different in comparison to mononuclear catalysts. Moreover, there are positive and negative types of the effects.[11,12,19–23,32,33]

As the synergistic and cooperative effects are a result of electronic, steric and multinuclear interactions, the structural parameters of the catalysts determine the level and mechanism of these effects. These parameters include the nature of the metal centers, distance between the active sites, structure of the spacer, probable catalyst stereoisomer as well as the length of the monomer or π-alkyl.[12,33–42] Interestingly, the presence of possible stereoisomers is one of the challenges that affect the multinuclearity effect and polymer properties obtained. In previous reports, the presence of different spatial stereoisomers for dinuclear olefin catalysts was presented.[36–44] The stability, fraction, selectivity and behaviour of each isomer depends on the structure and reaction conditions. However, the stereoisomers may have similar behaviour in comparison with mononuclear analogues when the centers are far from each other or the overall interactions do not favour cooperation. In addition, the agostic interaction between the monomer or macromonomer chain and the second metal center, considering the complex structure, has a substantial effect on the catalyst performance and polymer properties.

[a] *Department of Catalyst, Iran Polymer and Petrochemical Institute (IPPI), P.O. Box 14965/115, Tehran, Iran. E-mail: S.ahmadjo@ippi.ac.ir*
[b] *Department of Chemical and Materials Engineering, University of Alberta, Edmonton, Alberta T6G 1H9, Canada*
[c] *Department of Chemistry, Faculty of Science, Ferdowsi University of Mashhad, P.O. Box: 91775, Mashhad, Iran*

† Electronic supplementary information (ESI) available: Experimental and theoretical details are including optimized structures, ^{13}C NMR spectrums and chemical shift assignment and DSC thermograms. See DOI: 10.1039/c8nj04481c

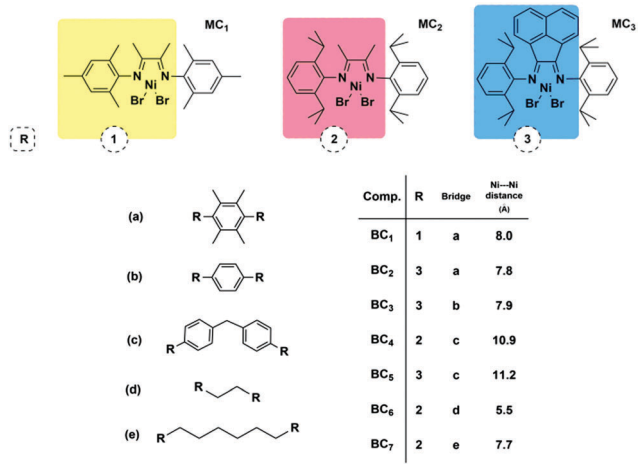

Comp.	R	Bridge	Ni---Ni distance (A)
BC_1	1	a	8.0
BC_2	3	a	7.8
BC_3	3	b	7.9
BC_4	2	c	10.9
BC_5	3	c	11.2
BC_6	2	d	5.5
BC_7	2	e	7.7

Scheme 1 Representative structures of mono- and dinuclear catalysts.

Through our recent studies that focused on the polymerization of α-olefins using a series of mono and dinuclear Ni α-diimine-based catalysts (Scheme 1), the average molecular weight and distribution have been reported.[45] As presented in these studies, the M_w and MWD of poly(1-hexene) samples with regard to catalyst structure could be varied. Based on this, the catalysts BC_3–BC_7 showed a broad to bi-modal distribution, while the catalyst BC_2 afforded higher molecular weight and virtually narrow MWD of poly(1-hexene) with the highest catalytic activity. Supplementary analysis on the microstructure and thermal properties of the samples along with the computational study on catalyst structure and plausible mechanism are discussed in the following sections. Moreover, the effects of polymerization parameters such as monomer type and concentration, cocatalyst nature, polymerization temperature and time were studied comprehensively.

Experimental

Materials

All manipulations of air/water-sensitive compounds were conducted under Ar/N_2 atmosphere using the standard Schlenk techniques. All solvents were purified prior to use. Toluene (purity 99.9%) was purified over sodium wire/benzophenone and used as polymerization media. Dichloromethane (purity 96%) (Sigma Aldrich Chemicals, Germany) and methanol (Merck chemical) were purified over calcium hydride powder and distilled prior to use in a complex and ligand synthesis as solvent. Xylene was purchased from Merck Chemical. 1-Hexene, 1-octene and 1-decene monomers were supplied by Aria Sasol petrochemical company. 2,4,6-Trimethylaniline, 2,6-diisopropylaniline, butanedione, 1,4-phenylenediamine, 2,3,5,6-tetramethyphenyldiamine, ethylenediamine, 1,6-hexanediamine, 4,4′-methylenedianiline, acenaphthoquinone, nickel(II) bromide ethylene glycol dimethyl ether complex [(DME)$NiBr_2$] (purity 97%) and diethyl ether (purity 99.5%) were supplied by Merck Chemical (Darmstadt, Germany) and used in the synthesis of ligands and catalysts. Diethylaluminum chloride (DEAC, 97% purity), ethylaluminum sesquichloride (EASC, 97% purity) and modified methylaluminoxane (MMAO, 7% in toluene) were supplied by Sigma Aldrich Chemicals (Steinheim, Germany).

Preparation of ligands and catalysts

The ligands and corresponding complexes (MC_n, n = 1–3 and BC_n, n = 1–7) were synthesized (Scheme 1) and fully described in our recent report.[45]

Polymerization procedure

The polymerization of α-olefin (purified prior to use) was performed in a round-bottom flask. Polymerization was conducted under Schlenk system. The monomer (10 mL) was injected into the round-bottom flask, which contained 10 mL toluene. Subsequently, the cocatalyst and catalyst were introduced into the flask, in sequence. The solution was stirred for a determined amount of time (12 or 24 h). In case of low or higher polymerization temperature, an ice or oil bath was used. Poly(α-olefin) was precipitated and purified by acidic methanol (5%) and dried under reduced pressure.

Characterization

^{13}C NMR and FT-IR spectra were obtained using Bruker AC-400 and Thermo Nicolet AVATAR 370 spectrometers, respectively. Intrinsic viscosity [η] was measured in toluene at room temperature using an Ubbelohde viscometer. M_v values were calculated according to the Mark-Houwink equation, $\eta = KM_v^{\alpha}$ (α = 0.69, $K = 2.28 \times 10^{-2}$).[33] Molecular weight distributions (MWDs) were determined with a Polymer Char high-temperature gel permeation chromatographer (GPC), which was operated at 145 °C using 1,2,4-trichlorobenzene under a flow rate of 1 mL min^{-1}. The GPC was equipped with three detectors in series (infrared, light scattering, and differential viscometer) and calibrated with polystyrene narrow standards. Differential scanning calorimetry (DSC) thermograms were recorded with a Perkin Elmer DSC Q100 instrument.

Results and discussion

Theoretical studies

Based on some literature reports and our previous reports, we suggested the presence of more than one active center, which was attributed to two possible stereoisomers of dinuclear catalysts formed during the production of broad to bimodal polymers. Furthermore, a series of theoretical calculations were performed. To pursue the changes in energies and interactions, we assumed the structures in three cases, namely, pre-catalysts, methyl cationic active centers and olefin π-complexes.[20,46–48] As the attempts to obtain crystals for the catalysts failed, we built the pre-catalyst structures at ground state *via* the DFT method at B3LYP level using the 6-31+G basis set, while the other structures were calculated at the excited state. All the structures in both *syn* and *anti* stereoisomers were optimized and compared. It was also disclosed that in the polymerization of α-olefins, the rate-determining step is monomer trapping,

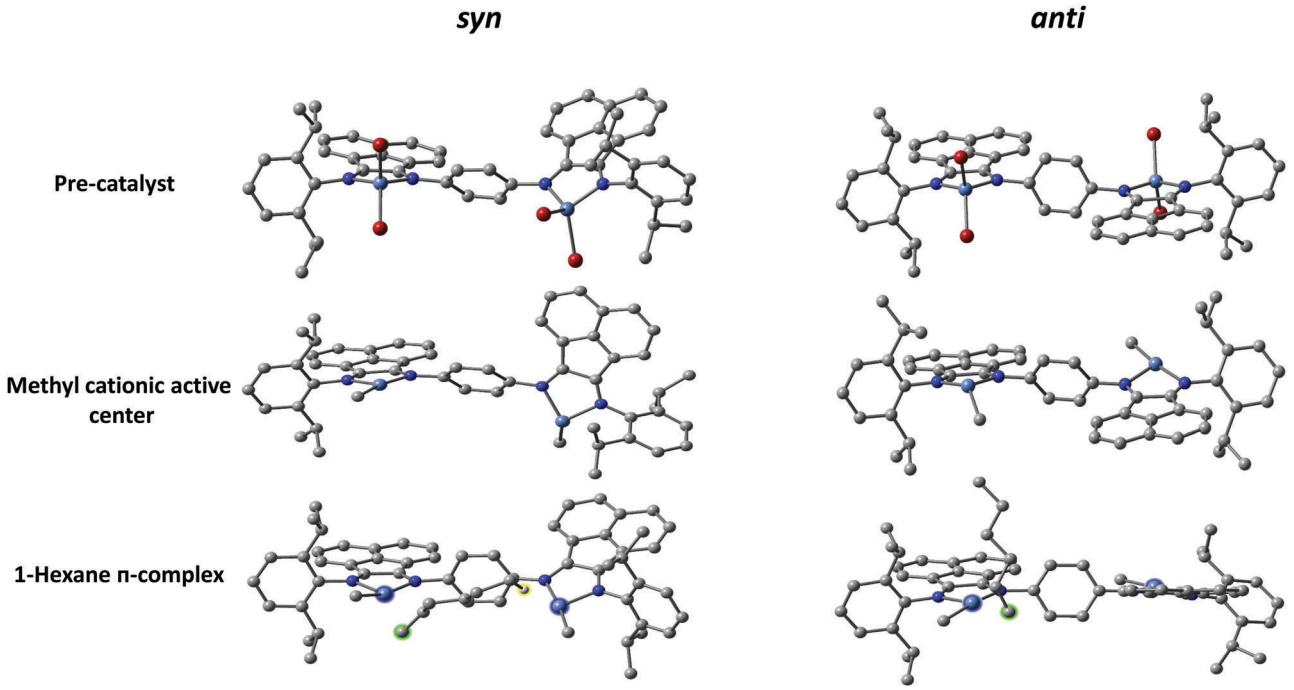

Fig. 1 Optimized stereoisomers precatalysts, methyl cationic active centers and 1-hexene π-complexes of BC_3 (hydrogen atoms are omitted for clarity).

which was considered to occur through π-complexes. As an example, the optimized structures for BC_3 catalyst are depicted in Fig. 1. (additional structures are provided in ESI,† Fig. S1–S6). Additional evidence for the presence of stereoisomers was determined in our previous reports, where polyethylene (PE) obtained by catalyst BC_3 showed a broad MWD (17.8).[20] Surprisingly, anchoring of the catalyst on the surface of nanographene through π–π stacking and electrostatic interactions resulted in a polymer with a narrow MWD (2.2).[49] This suggested that prohibiting the rotation by fixing could lead to one stereoisomer affording a unimodal MWD.

The *ortho*-aryl substituents in mononuclear catalysts have shown a huge impact on the activity and molecular weight and distribution of the polymer. In addition, in our dinuclear catalysts, these substituents had a key role in the interaction between stereoisomers and the catalytic species. It should be noted that the *ortho*-substituents on the bridge have an influence on the rotation of C–N single bond and the orientation of the metal centers in *syn* and *anti* isomers. As a result, the levels of energies for dinuclear catalyst structures (BC_1–BC_7) depend on the nature and length of the bridge and substituents, which determine the extent of the interactions. The theoretical results for precatalysts are gathered in Fig. 2. For BC_1 and BC_2, the results showed that the rotation to reach *syn* stereoisomer needs higher energy in precatalysts (>10 kcal mol^{-1}) and the *anti* stereoisomer is more stable than the *syn* stereoisomer. Interestingly, the *syn* form was the stable conformer for the catalysts BC_4–BC_7, and the required energy for rotation is less than 5 kcal mol^{-1} for all the BC_3–BC_7 precatalysts.

For precatalyst BC_3, the interval of stereoisomer energies is high, but it diminishes for the methyl cationic active species

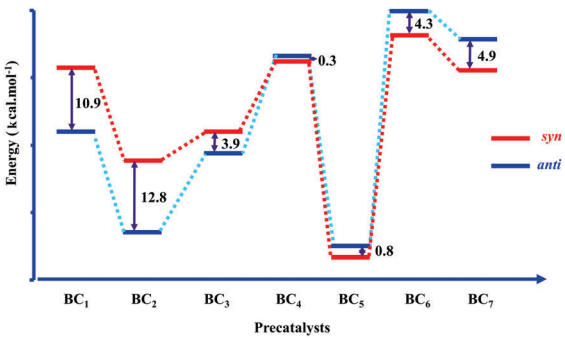

Fig. 2 Stability and energy barrier between the *syn* and *anti* stereoisomers.

and π-complexes (all graphs are provided in Fig. S7, ESI†). The differences in the potential energy of stereoisomers in the precatalyst state can decrease or change in activated cationic and π-complex species. The results of the energies, even in the cationic and π-complex species of two stereoisomers for BC_1 and BC_2, indicated that the intervals substantially decreased. The theoretical outputs with regard to the structure of the bridge could confirm the broadening of MWD through the presence of two types of active species converting into each other very easily. To clarify, each stereoisomer can polymerize the monomer to a low or high average molecular weight fraction. The initial results showed that in dinuclear catalysts with rigid structures on the bridge along with *ortho*-alkyl substituents, there was one stable isomer (BC_1 and BC_2), while for BC_3–BC_7, through flexibility on the bridge, both *syn* and *anti* stereoisomers could exist. These results also revealed that the presence of stereoisomers also may depend on the monomer

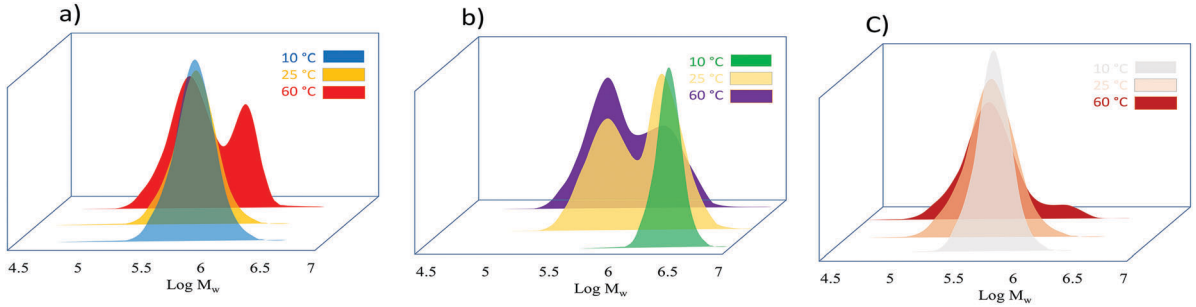

Fig. 3 GPC curves of (a) poly(1-hexene), (b) poly(1-octene) and (c) poly(1-decene) obtained by BC_2 at T_p = 10, 25 and 60 °C.

length and polymerization temperature.[38,40] Based on these results, poly(1-hexene) obtained at higher temperatures showed broader distribution.

It has been demonstrated that high polymerization temperature can provide the required energy for rotation. Moreover, the polymerization of longer α-olefins such as 1-octene and 1-decene suggested that the monomer length is another controlling factor.[38] For 1-octene, a strong agostic interaction (high local concentration of monomer) is responsible for producing the ultra-high molecular weight fraction (10, 25 and 60 °C), as confirmed from the molecular calculations (Fig. 3b).[11,45] In other words, the strong agostic interaction of hydrogen atom of the seventh carbon in 1-octene and the second metal center led to a high local concentration of monomer, high conversion and high molecular weight of poly(1-octene).[11,33,38] This interaction could also be observed in the energy intervals of *syn* and *anti* stereoisomers (≈9.1 kcal mol^{-1}), with the *syn* isomer being much more stable. Moreover, poly(1-decene) samples exhibited narrow MWD (≈1.7) due to the presence of only the *anti* stereoisomer (Fig. 3c). However, at higher temperatures, a broadening to bimodality of distribution was observed, which implied the presence of additional stereoisomers by providing the required energy for rotation of the *N*-aryl bond. The computational output showed that the energy interval of the *syn* and *anti* forms (2.9 kcal mol^{-1}) is close to that of the 1-hexene π-complex (3.2 kcal mol^{-1}) and the *anti* isomer is the stable form of 1-decene π-complex. However, a weak agostic interaction was observed for the 1-hexene π-complex between the H-alkyl and second Ni center in the *syn* form (Fig. S2 in ESI†). These observations can be attributed to the distance of the Ni centers in *syn* and *anti* stereoisomers and the overall electrostatic interaction of the monomer and centers; for 1-decene, the repulsion between the monomer-end and *ortho*-aryl substituents is stronger than the agostic interaction.

On deeply studying the GPC-IR graphs displayed in Fig. 4, the different trends can be observed for short chain branches (SCB). Each stereoisomer can be responsible for producing a low and high molecular weight fraction of the polymer. An increase or decrease in SCBs as a function of molecular weight represents the catalyst behavior with regard to the structure. For BC_1 and BC_2, the SCBs increased with the growth of molecular weights resembling mononuclear analogues. Moreover, lower SCB for BC_2 was obtained due to greater chain walking at higher M_w (*anti*). For the low molecular weight fraction of the polymer obtained by catalysts BC_3–BC_7, the changes in SCBs are the same except for BC_4, where the barrier energies in the precatalyst, methyl cationic active center and π-complex are minor. The higher molecular fraction might be attributed to the proximity of the centers and the consequent agostic interaction of the growing polymer chain, second Ni center and chain walking.

As the complex structure is very important to the catalyst behaviour and polymer properties, any changes in structure can lead to a different polymer architecture. This architecture with regard to possible mechanisms of α-olefin insertions and enchainment using some mononuclear α-diimine Ni catalysts has been discussed in the literatures.[16,50–56] To study the obtained poly(1-hexene) architecture, the branching density and distribution were determined by ^{13}C NMR and tabulated in Table 1. The chemical shifts, peak assignments and NMR spectra are provided in Table S1 and Fig. S8 (ESI†). Additional spectra are gathered in Fig. S9 and S10 (ESI†). Normally, insertion (1,2- or 2,1-) of 1-hexene monomer leads to butyl branching (no chain walking), while further branching types are a result of complete or partial chain walking, which is well described in the literature.[54] Partial chain walking results from a series of β-hydride elimination and reinsertion steps. In the case of 2,6-enchainment or chain walking, methyl and long chain branches are produced, although 1,6-enchainment affords a linear structure. The structural affinity for each insertion and partial or complete chain walking is a function of electronic and steric effects.[50–55] Although the behaviour of mononuclear catalysts with regard to chain walking is almost similar (Table 1 and Fig. 5), by increasing the steric and electronic effects of the backbone and *ortho*-aryl substituents on the ligand structure, the tendency of the catalyst towards normal insertion decreased from MC_1 to MC_3.[33,53,57] The 1,2-insertion values for dinuclears (BC_3–BC_7) could not be determined because selectivity of each stereoisomer as a single structure in regard to microstructure is not specific. Regiorandom insertions for mononuclear (MC_3) have also been presented in the literature.[50,54] From the bar chart in Fig. 4, it can be observed that the complete chain walking for BC_1 and BC_2 is high. This suggests that both *ortho*-aryl substituents and dinuclearity in BC_1 and BC_2 along with the optimum bulkiness in BC_2 are the reasons of this observation, which implies the stabilization of the electron-deficient and coordinatively unsaturated active intermediate.[53]

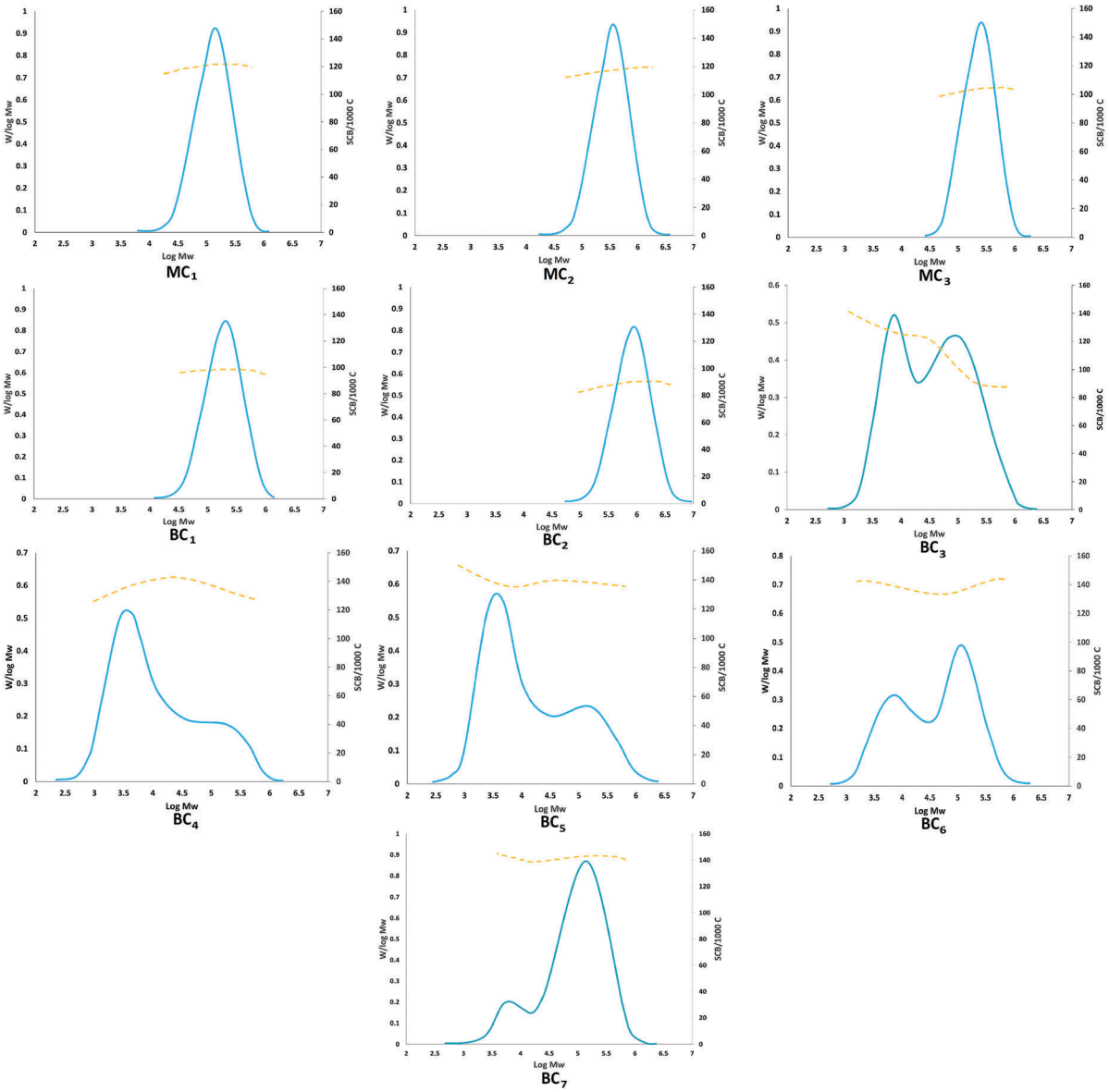

Fig. 4 GPC-IR graphs of poly(1-hexene) samples (dissolved in TCB at 145 °C) obtained by mono- and dinuclear catalysts.

Table 1 Branching distribution and thermal properties of the poly(1-hexene) samples[a]

			Branch distribution[b] (%)							
Entry	Cat.	BD[b] (1000 C)	Methyl	Ethyl	Propyl	Butyl	Long (>C$_4$)	T_g[c] (°C)	T_m[c] (°C)	ΔH[c] (J g^{-1})
1	MC$_1$	121.1	27.7	0	0	67.4	4.9	−57.5	—	—
2	MC$_2$	117.7	32.1	0	0	64.2	3.6	−56.6	—	—
3	MC$_3$	110.0	33.1	0	0	61.3	5.6	−55.4	−15.5	5.5
4	BC$_1$	98.5	42.7	0	2.7	43.3	11.3	−54.5	14	10.69
5	BC$_2$	96.9	28.1	2.5	7.8	49.0	12.6	−56.9	−8.3	12.98
6	BC$_3$	154.0	49.1	5.1	10.1	27.8	7.8	−68.1	−15.0	9.5
7	BC$_4$	136.5	58.9	10.2	16.5	12.5	1.9	−69.4	—	—
8	BC$_5$	149.4	47.9	14.7	18.4	12.1	6.8	−70.8	—	—
9	BC$_6$	141.6	41.3	14.1	18.5	18.9	7.2	−67.1	—	—
10	BC$_7$	147.2	44.9	16.0	14.2	17.3	7.6	−75.7	—	—

[a] Polymerization conditions: DEAC as cocatalyst, [Al]/[Ni] = 1500, [catalyst] = 3 μmol, room temperature (25 °C), polymerization time = 24 h, 10 cc toluene as solvent. [b] Determined using ^{13}C NMR spectroscopy. [c] Determined using differential scanning calorimetry (DSC).

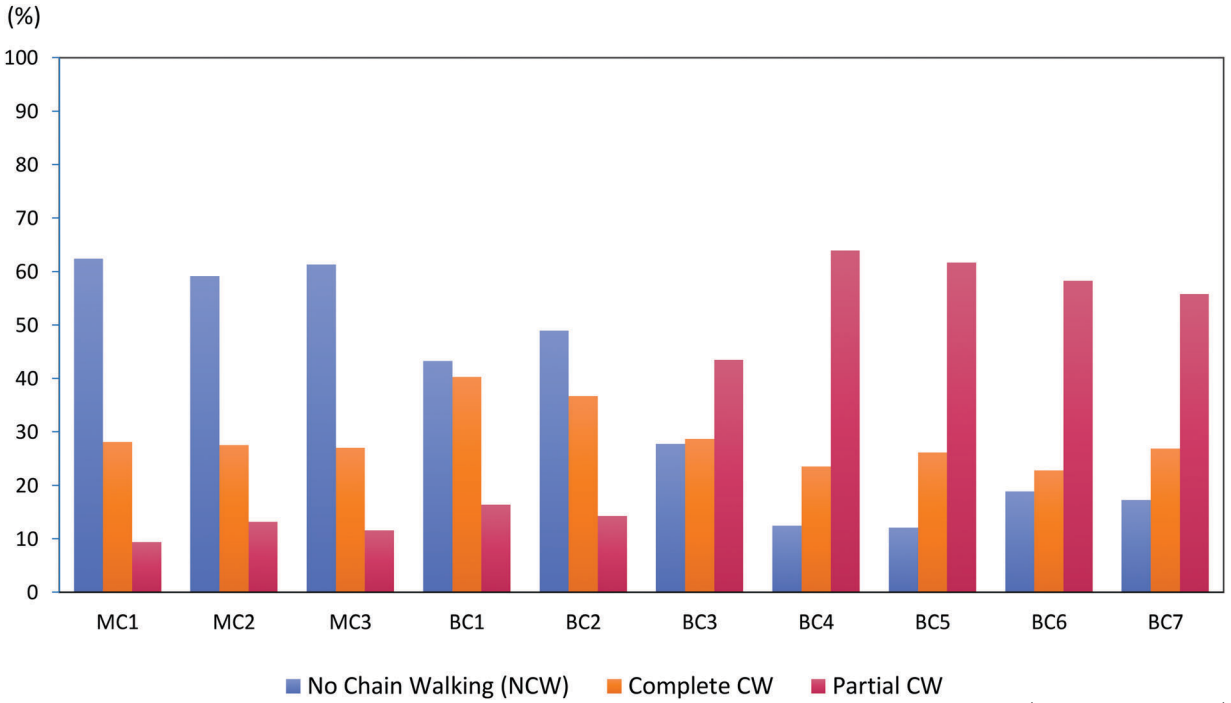

Fig. 5 Distribution of chain walking for mono- and dinuclear catalysts $\mathrm{NCW\%} = \left(\frac{\text{No. of butyl branches}}{\text{Total no. of branches}}\right) \times 100$, $\mathrm{PCW\%} = \left(\frac{\text{No. of ethyl} + \text{propyl} + \text{methyl} \times \text{branches}}{\text{Total no. of branches}}\right) \times 100$, CCW% = 100 − (NCW% + PCW%), calculated for peaks no. 5 and 25 in Table S1 (ESI†).

Further differences between the BC_1, BC_2 and mononuclear analogues (MC_1 and MC_3) are lower branching densities, presence of propyl branches and higher level of long chain branches (LCBs) ($>C_4$). In other words, the tendency of the dinuclear catalysts for chain walking (partial or complete) is greater than that of the mononuclears. Most interestingly, for the samples produced by BC_3–BC_7, in comparison with those produced by BC_1 and BC_2, there is greater branching content and diversity in branching distribution, where the high levels of ethyl and propyl branches were a result of partial chain walking. The chemical shifts at 11.10, 26.15 and 39.10 ppm indicate the ethyl branches, and peaks at 14.80, 20.05 and 35.90 are representative of the propyl branches (Fig. S9 and 10, ESI†). Moreover, the peaks at 27.8 ppm and 39–44 ppm are attributed to the presented microstructure (A–D) in Fig. 6. As we suggested earlier, the *anti* stereoisomer of the dinuclear catalysts (BC_n) favours 1,2-insertion and the subsequent pathways resembling mononuclear catalysts (MC_n). Furthermore, the *syn* stereoisomer,

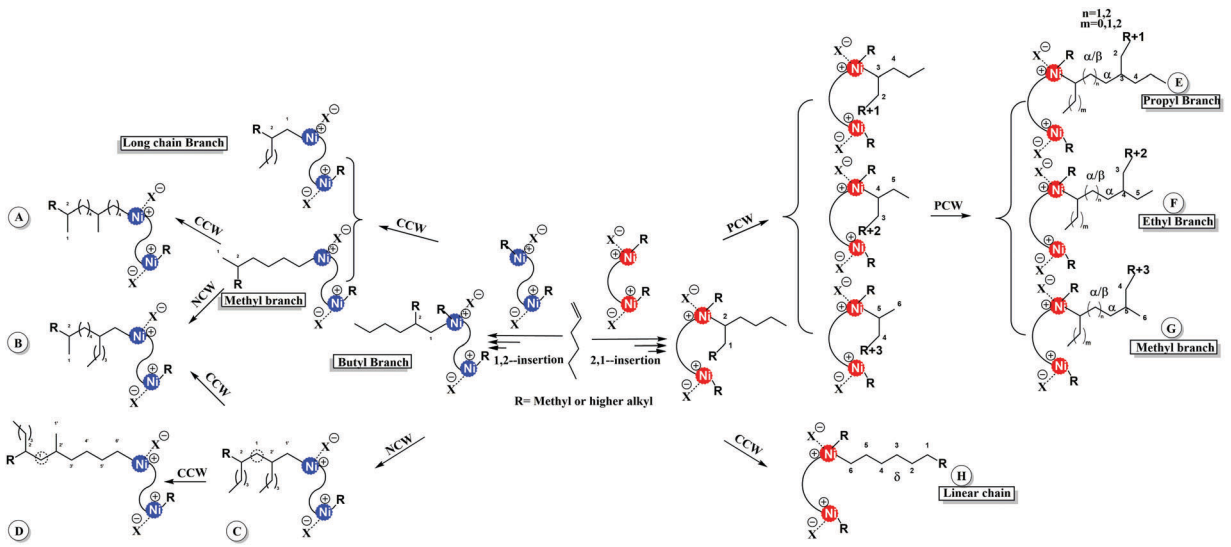

Fig. 6 The proposed mechanism for the polymerization of 1-hexene regarding the catalyst stereoisomers.

due to the dinuclearity effect and agostic interaction, favours 2,1-insertion of the monomer. This pathway can lead to E–G microstructures resulting from the partial chain walking mechanism and also H microstructure resulting from complete chain walking (Fig. 6).

The glass transition temperature (T_g), which is a function of chain mobility, revealed that higher level of chain branching as well as diversity in the distribution of branches led to higher chain mobility and lower T_g.[33] For mononuclear series, T_g increased as the mobility and branching distribution of the polymer chain decreased (Table 1 and Fig. S11, ESI†). Although in BC_1 and BC_2, the BDs are less than those of mononuclears, the diversity of branches are still high. Moreover, the higher linearity feature of the poly(1-hexene) samples represents the complete chain walking (chain straightening) by dinuclear catalysts and led to a broad melting area. The different domains of crystallinity in these samples are also the reason for the broadening of melting temperature (Fig. S11, ESI†).[33]

Overall, the high level of branching density and diversity of samples obtained by BC_3–BC_7 resulted in higher chain mobility and consequent lower T_g; the bar chart in Fig. 5 shows the catalyst behaviour with regard to the chain walking pathway. The behaviour of the dinuclear catalysts with regard to the microstructure, molecular weight distribution and SCBs are attributed to the dinuclearity and agostic interactions between hydrogen of the binding polymer chain and the second Ni center in the *syn* stereoisomer. The proposed mechanism for each stereoisomer is depicted in Fig. 6. The behaviour of dinuclear catalysts resembles mononuclears in *anti*-form. However, the *syn* stereoisomer favours a high level of 2,1-insertion and partial chain walking.

As it can be observed in Table 2, monomer conversions are low, which could be attributed to the low concentration of catalyst in the polymerization media. It has also been observed that the conversions for dinuclears were higher than those for mononuclear analogues, according to our recent report.[45] The effect of the cocatalyst type (DEAC, EASC and MMAO), [Al]/[Ni] molar ratios (1000–2000) and free solvent polymerization on catalyst behaviour and poly(1-hexene) properties were investigated (Table 2 and Fig. S12, S13, ESI†). There are two factors with regard to the nature of cocatalysts, including size and acidity, which are conducive to the rapid and improved alkylation of the metal complex.[49] In the BC_2/DEAC catalytic system, in comparison with BC_2/MMAO and BC_2/EASC, the branching density was lower. EASC as a stronger Lewis acid activated the metal center more efficiently, and the highest monomer conversion (49.5%) and branching density (133.5) and narrowest MWD (2.1) values were observed. MMAO, being larger in size than EASC and DEAC, allowed Ni to make LCBs ($>C_4$) and broad MWD (3.6). Changing the concentration of DEAC in the polymerization media had a high impact on the microstructure. Based on this, as the concentration of the DEAC increased, it induced the Ni center to go through partial chain walking and consequently create short chain branches. Higher density and diversity of branching also led to higher chain mobility and lower T_g with no significant melting temperature. Raising the concentration of monomer through the free solvent technique is one of the substantial polymerization parameters, which increased branching density, particularly for the butyl branches. This result can be attributed to the high level of conventional 1,2-insertion.[53] Moreover, the conversion percent increased due to the more accessible monomer at higher concentrations of 1-hexene around the active centers. Lower conversion ($\approx$5%) and molecular weight of 1-hexene was obtained when the polymerization was quenched after 12 h (entry 16, Table 2). The branching density increased, but the distribution did not show any significant difference with entry 5. Higher branching density data, according to the SCB curve in Fig. 4, for BC_2, which increases slightly with increasing M_w, indicate that BC_2, through lower tendency for chain walking, favours higher normal insertion.

The temperature, as it showed the impact on the catalyst isomerization, revealed a drastic influence on the poly(1-hexene) microstructure.[48,49] Based on this, the branching density decreased from 120.4 to 91.7/1000 C atoms as the temperature increased from 10 to 60 °C, while the SCBs increased. It can be concluded that the tendency of the catalyst for partial chain walking is a function of temperature and that the β-hydride elimination and also the reinsertion mechanism increases as the polymerization temperature rises. Furthermore, the glass transition temperature and melting area are also consistent with our previous results.[33]

Table 2 Microstructure properties of poly(α-olefin) samples produced by the catalyst BC_2 under different conditions[a]

					Branch distribution[b] (%)										
Entry	Cocat/[Al]/[Ni]	T_p (°C)	Con. (%)	BD[b] (1000 C)	Methyl	Ethyl	Propyl	Butyl	Long ($>C_4$)	T_g[c] (°C)	T_m[c] (°C)	ΔH[c] (J g^{-1})	M_v	M_w[d]	MWD[d]
11	DEAC/1000	25	16.6	109.5	29.3	0	7.3	54.3	9.2	−56.3	—	—	13.6	17.8	2.0
12	DEAC/2000	25	32.7	103.4	39.1	1.3	10.2	44.5	4.9	−57.6	—	—	11.3	12.2	2.3
13	DEAC/1500	10	22.8	120.4	25.4	0	4.1	60.3	10.2	−55.7	—	—	16.2	18.0	1.8
14	DEAC/1500	60	19.3	91.7	31.7	4.9	8.1	42.0	13.3	−58.1	−17.1	3.3	8.1	4.3	3.1
15[e]	DEAC/1500	25	39.2	123.7	25.9	0	5.0	58.7	10.3	−61.8	—	—	18.1	19.2	2.0
16[f]	DEAC/1500	25	32.4	101.2	27.6	1.3	9.1	50.1	11.9	−57.1	−7.8	7.1	11.2	12.6	1.9
17	MMAO/1500	25	10.5	112.6	19.0	0	2.5	65.2	13.3	−57.2	−12.4	5.7	4.8	5.3	3.6
18	EASC/1500	25	44.9	133.5	34.6	0.7	9.3	50.3	5.2	−67.5	10.5	0.5	1.9	2.5	2.1
19[g]	DEAC/1500	25	36.1	89.2	15.7	1.0	2.1	0.9	80.3	−55.4	14.2	13.75	18.4	29.3	4.2
20[h]	DEAC/1500	25	31.0	83.5	10.1	0	0	0	89.9	−54.1	28.1	25.25	10.5	14.2	1.7

[a] Polymerization conditions: DEAC as cocatalyst, [Al]/[Ni] = 1500, [catalyst] = 3 μmol, room temperature (25 °C), polymerization time = 24 h, 10 cc toluene as solvent. [b] Determined using ^{13}C NMR spectroscopy. [c] Determined using DSC. [d] Determined using GPC. [e] Free solvent. [f] 12 h. [g] 1-Octene. [h] 1-Decene.

The theoretic values of branching density for the poly(α-olefin) samples are 166.7, 125 and 100 per 1000 C atoms for poly-(1-hexene), poly(1-octene) and poly(1-decene), respectively. These values are in the case of normal insertion without any further enchainment or chain walking. The microstructure of the poly(α-olefins) obtained at 25 °C showed that for longer monomers, the branching density percent increases from 58 to 83% (Table 2 and Fig. S14, ESI†). In other words, the tendency of the catalyst for chain walking decreases as the monomer length increases. However, some SCBs ($\leq C_4$) were observed for poly(1-octene), which is evidence of partial chain walking. Furthermore, with regards to the broad MWD (Fig. 3), the presence of a higher *syn* stereoisomer fraction was confirmed. DSC thermograms of the samples illustrated higher T_g, T_m and melting area due to longer methylene (linear segment as a monomer chain length) units and lower chain mobility (Fig. S15, ESI†).[33,53] The conversion percent and molecular weight of the poly(α-olefin) samples decreased as the temperature increased to 60 °C. This can be attributed to the deactivation of catalyst and the increase in chain transfer reactions.[20,33] Furthermore, lower boiling point and decreased solubility of the solvent may imply the higher reduction rate for 1-hexene. Higher conversion of 1-octene in comparison with 1-hexene and 1-decene also implied strong agostic interaction that can increase the local concentration of 1-octene around the adjacent Ni center and lead to higher rate of propagation and higher molecular weight of the sample.

Conclusion

MWD broadening for dinuclear catalysts was attributed to the presence of different stereoisomers (*syn* and *anti*) according to the results of polymers made by all dinuclear catalysts. The stability, portion and behaviour of each stereoisomer depend on the catalyst structure including the rigidity, steric effect on the bridge and distance between the centers. Although high energy interval of stereoisomers in some dinuclear precatalyst structures affords one stable isomer, interconversion during polymerization could easily occur. Moreover, polymerization parameters such as monomer length and temperature had an influence on the catalyst behaviour with regard to agostic interactions and kinetic energy. The results also suggested that each stereoisomer could have a different polymerization pathway. Partial chain walking as the main route for producing ethyl and propyl branches in poly(α-olefin) microstructure could be obtained *via* a flexible spacer between the centers in a confined distance. In contrast, higher levels of complete chain walking are observed due to higher electronic and steric effects on the backbone and bridge. The computational study confirmed the experimental results and revealed that the energy intervals between the three cases (precatalysts, methyl cationic active centers and α-olefin π-complexes) for both stereoisomers could be a good measure of catalyst structure and stability. Moreover, cocatalyst nature and concentration played key roles in the microstructure properties, where the EASC was a more effective activator to yield poly(1-hexene) with broader MWD. As monomer conversion increased with time, the polymerization temperature showed an optimum value (25 °C) along with the impact on catalyst behaviour (higher chain walking and interconversion). Free solvent polymerization due to a high concentration of accessible monomer for the active center led to higher conversion, M_w, normal insertion and narrow MWD. In addition to a high level of branching density, the diversity of the branches in the microstructure of poly(α-olefin) afforded greater chain mobility and lower T_g.

Conflicts of interest

There are no conflicts to declare.

Acknowledgements

The authors are thankful to University of Alberta (U of A), Iran Polymer and Petrochemical Institute (IPPI) and Ferdowsi University of Mashhad (FUM) for all of their cooperation.

Notes and references

1 C. Chen, *ACS Catal.*, 2018, **8**, 5506–5514.
2 C. Chen, *Nat. Rev. Chem.*, 2018, **2**, 6–14.
3 S. Zhou and C. Chen, *Sci. Bull.*, 2018, **63**, 441–445.
4 M. Li, X. Wang, Y. Luo and C. Chen, *Angew. Chem., Int. Ed.*, 2017, **56**, 11604–11609.
5 M. Zhao and C. Chen, *ACS Catal.*, 2017, **7**, 7490–7494.
6 L. Guo, C. Zou, S. Dai and C. Chen, *Polymers*, 2017, **9**, 122.
7 C. Zou, S. Dai and C. Chen, *Macromolecules*, 2017, **51**, 49–56.
8 Y. Na, S. Dai and C. Chen, *Macromolecules*, 2018, **51**, 4040–4048.
9 S. Dai and C. Chen, *Macromolecules*, 2018, **51**, 6818–6824.
10 J. Fang, X. Sui, Y. Li and C. Chen, *Polym. Chem.*, 2016, **9**, 4143–4149.
11 M. Delferro and T. J. Marks, *Chem. Rev.*, 2011, **111**, 2450–2485.
12 J. P. McInnis, M. Delferro and T. J. Marks, *Acc. Chem. Res.*, 2014, **47**, 2545–2557.
13 E. T. Kiesewetter and R. M. Waymouth, *Macromolecules*, 2013, **46**, 2569–2575.
14 P. D. Hyde and M. A. Craton, *US Pat.*, 6544643, 2003.
15 S. Ahmadjo, *Polym. Adv. Technol.*, 2016, **27**, 1523–1529.
16 G. Leone, M. Mauri, I. Pierro, G. Ricci, M. Canetti and F. Bertini, *Polymer*, 2016, **100**, 37–44.
17 F. Wang, R. Tanaka, Q. Li, Y. Nakayama and T. Shiono, *Organometallics*, 2018, **36**, 1358–1367.
18 M. P. Weberski, C. Changle, M. Delferro and T. J. Marks, *Chem. – Eur. J.*, 2012, **18**, 10715–10732.
19 M. Khoshsefat, G. H. Zohuri, N. Ramezanian, S. Ahmadjo and M. J. Haghpanah, *J. Polym. Sci., Part A: Polym. Chem.*, 2016, **18**, 3000–3011.
20 S. Liu, A. Motta, A. R. Mouat, M. Delferro and T. J. J. Marks, *Am. Chem. Soc.*, 2014, **136**, 10460–10469.

21 G. Tian, B. Wang, S. Xu, X. Zhou, Bo. Liang, L. Zhao, F. Zou and Y. Li, *Macromol. Chem. Phys.*, 2002, **203**, 31–36.
22 M. R. Salata and T. J. Marks, *Macromolecules*, 2009, **42**, 1920–1933.
23 F. Zhai and R. F. Jordan, *Organometallics*, 2017, **36**, 2784–2799.
24 D. N. Vaccarello, K. S. O'Connor, P. Iacono, J. M. Rose, A. E. Cherian and G. W. Coates, *J. Am. Chem. Soc.*, 2018, **140**, 6208–6211.
25 L. Guo, W. Liu and C. Chen, *Mater. Chem. Front.*, 2017, **1**, 2487–2494.
26 S. Dai, S. Zhou, W. Zhang and C. Chen, *Macromolecules*, 2016, **49**, 8855–8862.
27 K. Lian, Y. Zhu, W. Li, S. Dai and C. Chen, *Macromolecules*, 2017, **50**, 6074–6080.
28 S. Dai, X. Sui and C. Chen, *Angew. Chem., Int. Ed.*, 2015, **54**, 9948–9953.
29 S. Han, E. Yao, W. Qin, S. Zhang and Y. Ma, *Macromolecules*, 2012, **45**, 4054–4059.
30 H. Makio, H. Terao, A. Iwashita and T. Fujita, *Chem. Rev.*, 2011, **111**, 2363–2449.
31 H. Li, C. L. Stern and T. J. Marks, *Macromolecules*, 2005, **38**, 9015–9027.
32 S. Zhang, Q. Xing and W. H. Sun, *RSC Adv.*, 2016, **6**, 72170–72176.
33 A. Dechal, M. Khoshsefat, S. Ahmadjo, S. M. M. Mortazavi, G. H. Zohuri and H. Abedini, *Appl. Organomet. Chem.*, 2018, **32**, e4355.
34 M. H. Lee, S. K. Kim and Y. Do, *Organometallics*, 2005, **24**, 3618–3620.
35 H. Alshammari and H. G. Alt, *US Pat.*, 14002910, 2014.
36 S. Sujith, D. J. Joe, S. J. Na, Y. W. Park, C. H. Chow and B. Y. Lee, *Macromolecules*, 2005, **38**, 10027–10033.
37 C. Sierra, J. D. Hüerländer, M. Hill, G. Kehr, G. Erker and R. Fröhlich, *Chem. – Eur. J.*, 2003, **9**, 3618–3622.
38 S. Liu, A. M. Invergo, J. P. McInnis, A. R. Mouat, A. Motta, T. L. Lohr, M. Delferro and T. J. Marks, *Organometallics*, 2017, **36**, 4403–4421.
39 R. E. Murray, K. C. Jayaratne, Q. Yang, J. L. Martin and G. L. Glass, *US Pat.*, 7919639, 2011.
40 M. R. Radlauer, M. W. Day and T. Agapie, *Organometallics*, 2012, **31**, 2231–2243.
41 Z. Chen, E. Yao, J. Wang, X. Gong and Y. Ma, *Macromolecules*, 2016, **49**, 8848–8854.
42 Z. Chen, X. Zhao, X. Gong, D. Xu and Y. Ma, *Macromolecules*, 2017, **50**, 6561–6568.
43 Y. Na, X. Wang, K. Lian, Y. Zhu, W. Li, Y. Luo and C. Chen, *ChemCatChem*, 2017, **9**, 1062–1066.
44 S. Takano, D. Takeuchi and K. Osakada, *Chem. – Eur. J.*, 2015, **21**, 16209–16218.
45 M. Khoshsefat, S. Ahmadjo, S. M. M. Mortazavi, G. H. Zohuri and J. B. P. Soares, *New J. Chem.*, 2018, **42**, 8334–8337.
46 J. Ramos, A. Muñoz-Escalona and V. Cruz Martínez-Salazar, *J. Polym.*, 2003, **44**, 2177–2186.
47 D. A. C. Ferreira, de A. SaraF, S. M. P. Meneghetti and M. R. Meneghetti, *J. Mol. Catal. A: Chem.*, 2012, **363**, 1–9.
48 J. Ramos, V. L. Cruz, J. Martínez-Salazar, M. Brasse, P. Palma and J. Campora, *J. Polym. Sci., Part A: Polym. Chem.*, 2010, **48**, 1160–1165.
49 E. F. McCord, S. J. McLain, L. T. J. Nelson, S. D. Ittel, D. Tempel, C. M. Killian, L. K. Johnson and M. Brookhart, *Macromolecules*, 2007, **40**, 410–420.
50 H. Hu, H. Gao, D. Chen, G. Li, Y. Tan, G. Liang, F. Zhu and Q. Wu, *ACS Catal.*, 2014, **5**, 122–128.
51 F. Liu, H. Gao, Z. Hu, H. Hu, F. Zhu and Q. Wu, *J. Polym. Sci., Part A: Polym. Chem.*, 2012, **50**, 3859–3866.
52 I. Pierro, G. Zanchin, E. Parisini, J. Martí-Rujas, M. Canetti, G. Ricci, F. Bertini and G. Leone, *Macromolecules*, 2018, **51**, 801–814.
53 K. S. O'Connor, J. R. Lamb, T. Vaidya, I. Keresztes, K. Klimovica, A. M. LaPointe, O. Daugulis and G. W. Coates, *Macromolecules*, 2017, **50**, 7010–7027.
54 J. Sun, F. Wang, W. Li and M. Chen, *RSC Adv.*, 2017, **7**, 55051–55059.
55 J. D. Azoulay, G. C. Bazan and G. B. Galland, *Macromolecules*, 2010, **43**, 2794–2800.
56 J. Merna, Z. Hoštálek, J. Peleška and J. Roda, *Polymer*, 2009, **21**, 5016–5123.
57 M. Khoshsefat, S. Ahmadjo, S. M. M. Mortazavi and G. H. Zohuri, *RSC Adv.*, 2016, **6**, 88625–88632.

